Forces in Mechanics 10 (2023) 100166

Contents lists available at ScienceDirect

Forces in Mechanics

journal homepage: www.sciencedirect.com/journal/forces-in-mechanics

Investigating the role of different components of friction stir welding tools on the generated heat and strain☆

M. Akbari [a,*], M.R.M. Aliha [b], F. Berto [c]

[a] Department of Mechanical Engineering, Technical and Vocational University (TVU), Tehran, Iran
[b] Welding and Joining Research Center, School of Industrial Engineering, Iran University of Science and Technology (IUST), Narmak, 16846-13114,Tehran, Iran
[c] Department of Mechanical and Industrial Engineering, Norwegian University of Science and Technology (NTNU), Trondheim, Norway

ARTICLE INFO

Keywords:
Friction stir welding
Tool
Shoulder
Probe
Strain

ABSTRACT

Temperature and strain in friction stir welding (FSW) induced by the FSW/FSP tool play a critical role in successful welding. In order to properly design the FSW/FSP tool, it is necessary to understand the role of each component of the probe and shoulder of the tool in heat and strain generation. In this study, the heat and strain generated by the tool were numerically modeled using a thermo-mechanically coupled 3D FEM model. To investigate the effect of tool probe and shoulder on heat and strain production, a tool without a probe, a tool without a shoulder, and a complete tool were modeled, and the contribution of each component in heat and stress production was calculated. The results show that, in contrast to plastic deformation, frictional heat generation is the main mechanism for increasing workpiece temperature. Also, about 90% of the heat is generated by the tool shoulder, and the tool pin alone is not able to generate heat and strain in the samples.

1. Introduction

The majority of manufactured casting materials come from a class of materials called aluminum-silicon (Al-Si) alloys. These alloys are widely employed in aerospace and automobile industries due to their high strength-to-weight ratio, excellent wear resistance, and excellent castability [1,2]. This is caused by the alloy's favorable wear, corrosion resistance, and high castability. In particular, welded components have a weight reduction of 10% compared to mechanically fastened components and a cost reduction of up to 30% compared to numerical control machining and mechanical fastening [3]. However, when applied to various Al alloys, conventional welding techniques have several drawbacks that have occasionally deterred the usage of such welded products.

FSW is a popular solid-state joining method for bonding aluminum alloys. FSW welding prevents melting-related flaws because no material melts throughout the process [4,5]. The FSW technique was developed by Welding Institute in 1991. FSW/FSP causes significant plastic deformation and produces frictional heat. The temperature inside the workpiece increased as a result of both of these elements. The microstructure, including grain size and boundary features and the resulting mechanical properties of the joints, are significantly influenced by the temperature history during FSW/FSP. The thermal expansion coefficient of an alloy decreases with the amount of silicon it contains, reducing any shrinking that may occur during solidification.

During the FSW process, temperature generation and its distribution over various regions have a stimulating effect on the microstructural and mechanical characteristics of the manufactured welds. In order to achieve a better quality weld, researchers have done a lot of research on the study of temperature and strain during FSW. Ghiasvand et al. [6] studied the effects of the FSW probe offset and the position of dissimilar alloys on the peak temperature of FSW of AA5086 and AA6061 alloys. To calculate the peak temperatures produced while using FSW tools with four different probe profiles, Dhanesh Babu et al. [7] developed a thermomechanical process model. The goal was to understand better how these temperatures impacted their mechanical strength, grain size, and the joints' quality.

The analytical model's capacity to collect the necessary information

☆ The authors whose names are listed immediately below certify that they have NO affiliations with or involvement in any organization or entity with any financial interest (such as honoraria; educational grants; participation in speakers' bureaus; membership, employment, consultancies, stock ownership, or other equity interest; and expert testimony or patent-licensing arrangements), or non-financial interest (such as personal or professional relationships, affiliations, knowledge or beliefs) in the subject matter or materials discussed in this manuscript.

* Corresponding author.
E-mail address: mo-akbari@tvu.ac.ir (M. Akbari).

https://doi.org/10.1016/j.finmec.2023.100166
Received 8 December 2022; Received in revised form 3 January 2023; Accepted 3 January 2023
Available online 4 January 2023

for accurate quantitative prediction of the heat produced in the tool and the workpiece is hampered by the complexity of the thermal behavior of FSW. The analytical model is unable to adequately capture the necessary features for a quantitative forecast of the amount of heat generated in the tool and workpiece due to the complexity of the thermal behavior of FSW. As a result, FEM is recognized as a viable tool to resolve the challenging governing equations and thoroughly investigate the process. As evidenced by the enormous volume of published research works on the thermal analysis of FSW throughout the last decade, finite element modeling is a particularly suitable approach for modeling the FSW process. The coupled Eulerian-Lagrangian (CEL) approach was used by Akbari et al. [8] to simulate material mixing and SZ formation during the FSLW of brass and aluminum. The developed model accurately predicts the creation of the stir zone and material mixing at the Al/brass interface. Akbari and Asadi [9] developed a finite element model utilizing a coupled Eulerian-Lagrangian (CEL) technique to explore frequently occurring faults in the FSW process. The numerical model is generally designed to forecast a variety of defects, including inappropriate substrate joining, tunnel defect generation, excessive flash, voids, and other surface abnormalities. Using the finite element method, Akbari and Asadi [9] considered the flow of material and temperature profile during the in-process cooling FSP under various circumstances. To forecast temperature fluctuations during the dissimilar joining of AA5083 and AZ31 by FSW, Ranjole et al. [10] created a 3D FEM model. The findings showed that an increase in tool rotational speed had a greater impact on induced temperature than an increase in traverse speed. In this study, to investigate the effect of different tool components on the strain, temperature, and material flow, FSW/FSP was numerically simulated using rigid-viscoplastic 3D FEM.

The tool used for FSW consists of a particular shoulder and a probe with a specific profile that will be used to obtain the joints between the two sheets. This tool's shoulder will touch the top surface of the material after being forced to penetrate into the joining areas of the two workpieces at high speed. The tool is then designed to move along the joint line. Designing a suitable tool for joining metals with the FSW method is one of the key parameters in achieving a joint with appropriate microstructural and mechanical properties. So far, much research has been done to design suitable tools for the process. Most of these articles have studied the effect of tool probe shape [11–13], shoulder and tool probe diameter [14–16], tool probe length [16,17], and tool material [18]. Although much research has been carried out in the field of thermal and strain history investigation during the FSW process, none has determined the contribution of different tool components (probe and tool shoulder) in heat and strain generation. Determining the role of each component of the tool during the process will increase the knowledge of the process and improve the tool's design. For this reason, a tool without a probe, a tool without a shoulder, and an FSW tool were modeled, and the contribution of each component in heat and strain production was calculated.

2. Experimental method

Al-Si as-cast aluminum alloy plates with a 6 mm thickness were used for the experiments. Table 1 lists the chemical compositions of the alloys. At a temperature of 25 °C, all tests were conducted.

Fig. 1 displays the tool's dimensions and specifications. Table 2 also shows the mechanical and physical properties of A356.

A four channels thermometer with a 0.1 °C precision was utilized to record the temperature history during the FSW/FSP. The temperature in the translational zone was measured using four k-type thermocouples to validate the numerical model.

Table 1
Chemical compositions of aluminum alloy used in this research (wt %).

Si	Fe	Mn	Cu	Zn	Ti	Mg
7	0.31	0.1	0.2	0.1	0.25	0.3

3. FEM simulation of FSW

Due to its capacity to simulate extreme plastic deformation, Deform-$3D_{TM}$ software was employed for modeling thermal history, strain, and material flow during FSW/FSP [19,20]. Additionally, the tool and the workpiece were constructed of rigid viscoplastic materials. The following presumptions were made in this investigation to help simplify the problem:

1- The FSW/FSP tool's and workpiece's thermal characteristics are considered constant (Table 2).
2- The backing plate and the workpieces' two sides were fixed together.
3- At the ambient temperature of 20 C, there was free convection occurring on all free surfaces.

The friction between the samples and FSW/FSP tool was modeled using the constant shear friction model [19,21]:

$$f = mk \tag{1}$$

Where f is the frictional stress, k represents the shear yield stress, and m is the friction factor.

The tool and workpiece were meshing in a non-uniform manner with automatic re-meshing (Fig. 2). The smaller elements, with a mean size of 0.7 mm, were positioned beneath the tool probe. A detailed description of the FEM model can be found in our previous publications [22–29].

For all weldment surfaces in this investigation, the convective boundary condition is given as follows:

$$k\frac{\partial T}{\partial n} = h(T - T_{amb}) \tag{2}$$

Where h, $T_{amb,}$ and n represent the convection coefficient, the ambient air temperature, and the boundary's normal vector. The surfaces of the joints exposed to the atmosphere are given a convection coefficient of 20 W/(m^2. °C). Additionally, Table 3 summarizes the thermal characteristics of the workpiece and FSW/FSP tool.

In order to investigate the capability of the model in predicting the process, the developed model was validated. The experimental and simulation results are in good agreement with the comparison of temperature histories derived from the experimental and simulation (Fig. 3).

4. Result and discussion

4.1. Role of tool components component on temperature

The microstructure, material flow, and resulting mechanical characteristics are altered by the temperature history during FSW/FSP. It is well known that frictional heat between the workpiece and tool, combining, softening, and extrusion action of a revolving tool, are the methods used to join materials during the FSW/FSP. The FSW/FSP method must produce enough friction heat to maintain the material in a well-plasticized state at an adequate temperature in order to produce fine microstructure in SZ. In FSW/FSP, heat is produced as a result of plastic deformation surrounding the revolving tool as well as friction between the tool and the plate.

The latter is influenced by the friction area and friction factor between the workpiece and workpiece surface, as well as by the pressure applied to the tool and the welding head probe's rate of rotation.

Although the role of these two mechanisms in heat production is well known, the extent of their role has not been studied so far. In this research, in order to better understand the effect of each mechanism on heat production, two models were simulated. In the first model, zero friction was considered to calculate the heat generated due to plastic deformation. In the second model, the conversion rate of plastic work to heat was considered zero to calculate the amount of frictional heat

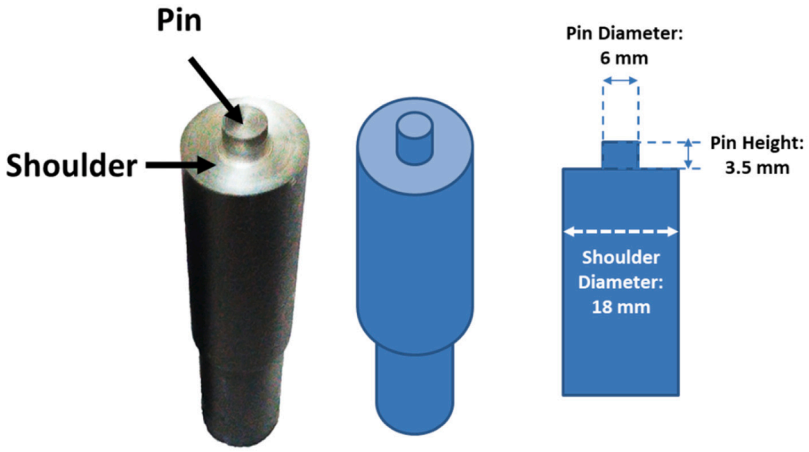

Fig. 1. The dimensions of the tools used in this research.

Table 2
Mechanical and physical properties of the A356.

Density	2.6 g/cm^3
Elastic Modulus	70 GPa
Yield Tensile Strength	120 MPa
Ultimate Tensile Strength	180 MPa
Hardness	44 HV

(Fig. 4).

As seen in Fig. 4, the increase in temperature in the workpiece is mainly due to heat generation due to the friction between the tool and the workpiece. The temperature increase caused by frictional heat is about 270°, which is more than three times the temperature increase due to plastic deformation. This analysis shows that frictional heat generation is the dominant mechanism in increasing workpiece temperature compared to plastic deformation.

The temperature distribution of the joints made using the FSW/FSP tool, the shoulderless tool, and the probe-less tool is shown in Fig. 5 along the transverse section. Because rotational speed—which is substantially higher than welding speed—dominates heat generation during the process, the temperature distribution around the centerlines of the joints is essentially symmetrical. Compared to joints made with

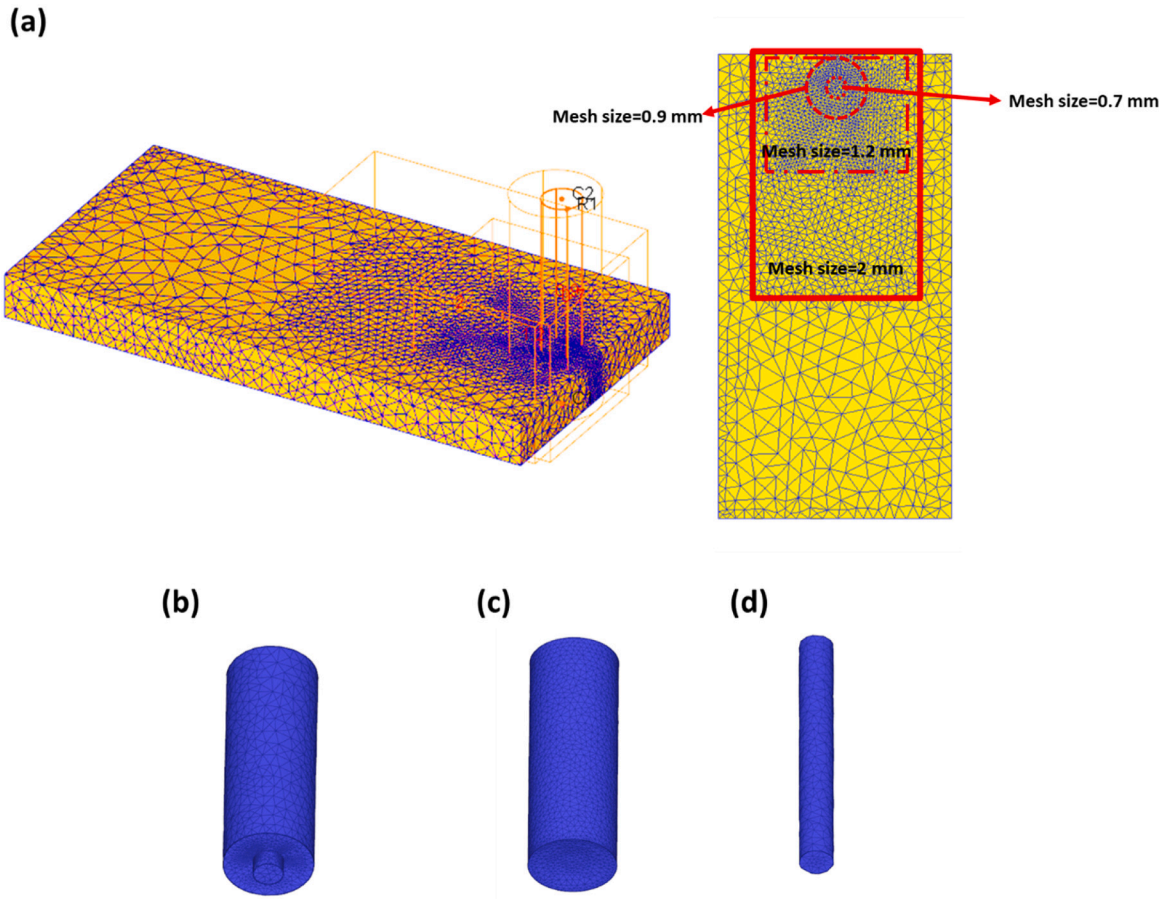

Fig. 2. Meshing of (a) workpieces, (b) FSW tool, (c) probless tool, (d) Shoulderless tool.

Table 3
Thermal properties of the aluminum alloy and H13 FSW/FSP tool.

Property	A356	FSW/FSP Tool
Heat capacity (N/mm^2°C)	2.57	4.5
Heat transfer coefficient between FSW tool and joint (N/ °C s mm2)	11	11
Conductivity (W/m °C)	117	24.5
Heat transfer coefficient between joint and backing plate (N/ C s mm)	5	

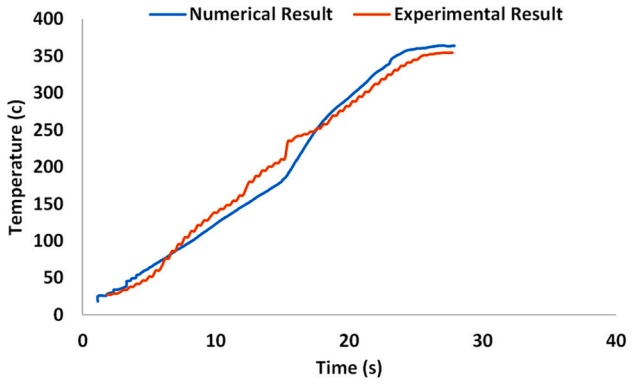

Fig. 3. Comparing the temperature history of the process obtained from experimental tests and numerical analysis.

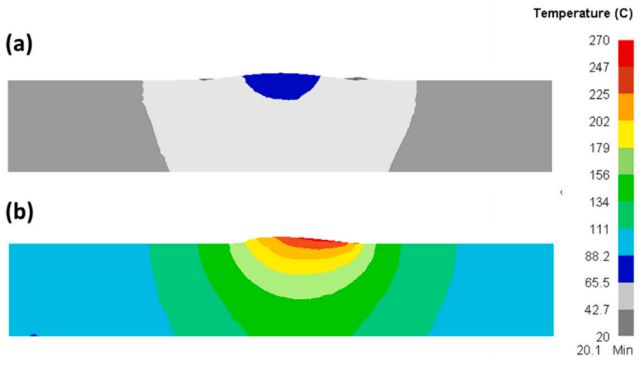

Fig. 4. Temperature increase in the material due to (a) Plastic deformation (b) Frictional heat.

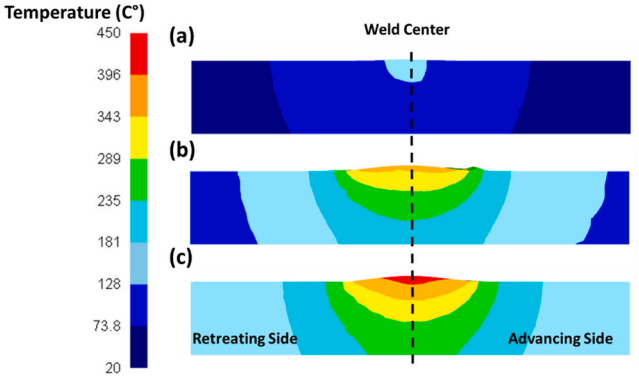

Fig. 5. Temperature changes in the cross-section of joints produced with (a) shoulderless tool, (b) probeless tool, (c) FSW tool.

shoulderless and probeless tools, the temperature of the joints made with the FSW/FSP tool is higher. The maximum temperature in the joint produced with the FSW/FSP tool is about 450°, and the maximum temperature in the joint produced with the probeless tool is 390°, which is about 90% of the temperature of the joint produced with the FSW/FSP tool. As can be seen, the temperature in the joint prepared with the probeless tool is slightly lower than that of the FSW/FSP tool, which indicates that the tool shoulder generates most of the heat generated. The temperature is much lower in the joint produced with the shoulderless tool than in the joint produced with the FSW/FSP tool, and this increase in temperature can only be seen around the probe. This analysis shows that the profile of the tool shoulder achieves the temperature of the workpiece, and the profile of the pin does not have much effect on the temperature of the workpiece.

4.2. Role of tool components on strain generation

Since it is evident that the plastic deformation and thermal history of the weld region have a significant impact on the weld's microstructure, a better understanding of how processing parameters affect the strain distribution in the weld during the FSW/FSP is very beneficial for process control and optimal design.

Fig. 6 shows the strain distribution during friction stir welding with the FSW/FSP, shoulderless, and probeless tools. The strain distributions around the weld line are not symmetrical, as can be seen in this figure. Additionally, the area impacted by strain is larger on the advancing side, where a "positive" interaction between the welding speed and tool rotational speed is apparent. In the joint produced with the FSW/FSP tool, the strain is much higher than the joints produced with the shoulderless and the probeless tool due to the combination of the effect of the tool probe and the shoulder. Also, the resulting strain can be divided into two strain areas caused by the shoulder and the strain caused by the tool's probe. The first zone, which is more near the joint's top surface, is the shoulder-affected zone, where the tool shoulder significantly impacts the material strain during the process. The second

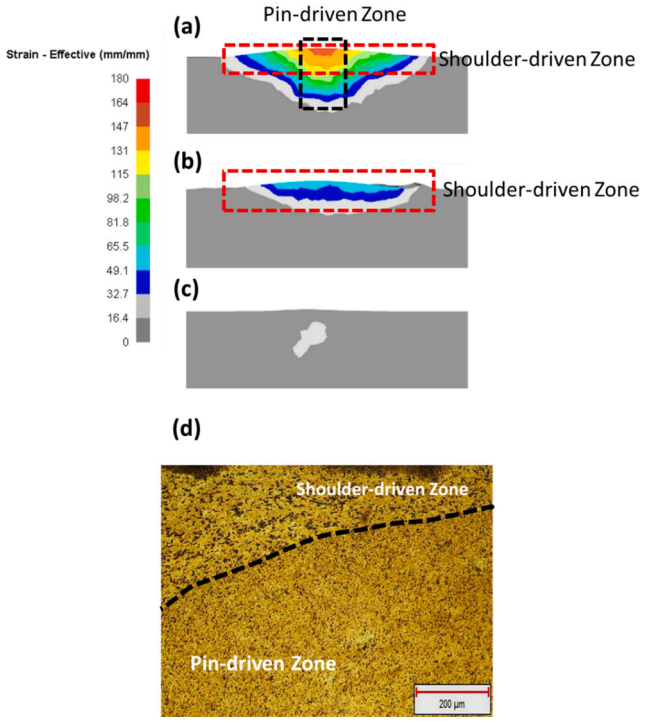

Fig. 6. Strain changes in the cross-section of samples produced with (a) shoulderless tool, (b) probeless tool, (c) FSW tool, (d) the microstructure of shoulder-affected zone.

zone where the cylindrical probe predominately influences material strain is known as the probe-affected zone. As it is known, the maximum strain occurs at the intersection of the area under the influence of the probe and under the influence of the shoulder. In this area, due to the combination of the effect of tool shoulder and tool probe in the material flow, the strain is higher than in other areas. In the sample without a probe, as it is known, strain is observed only in the area affected by the shoulder, which is much less than the FSW/FSP tool. In the FSW/FSP sample using a shoulderless tool, as it is known, there is only the area affected by the probe, where the strain is minimal. This small value shows that in the tool without a shoulder, the tool's probe cannot produce strain in the material. Due to insufficient heat generation by the shoulder of the tool, the material was not softened, and the shoulderless tool was unable to create strain in the material. These results show that the combination of the shoulder and probe effect causes strain and material flow in both areas under the influence of the shoulder and probe of the tool. The shoulder causes the temperature to increase and the material becomes soften, and the pin of the tool causes the material to flow and create strain. Without the tool shoulder, the temperature did not rise and the material flow did not form, and as a result, the materials experience very little strain. Also, without the tool pin, the material flow is formed only on the upper surface of the sheet due to the rotation of the tool shoulder.

Fig. 6 depicts the microstructure of the sample at the probe and shoulder-affected zones. It is evident that the size of the silicon particles in the shoulder-affected zone is more significant than those in the probe-affected zone. The Si particle size fluctuation from the shoulder-affected zone to the probe-affected zone may be caused by the higher produced temperature at the shoulder-affected zone. As the temperature rises, the material softens, leading to an increase in the strain that causes a reduction in the breakdown of silicon particles because it is now more straightforward for the Si particles to flow with the flow of the material without breaking.

The strain values divide the welding zone into three separate zones, namely SZ, TMAZ, and HAZ, according to the size of the silicon particles (Fig. 7). The coarse Si particles were broken up in the central areas of the weld, where the highest amount of strain occurs, and the silicon particles were uniformly dispersed in the stir zone. By moving away from the center line of the weld, the strain decreases, and the TMAZ region begins, where the size of the silicon particles is larger than the SZ region. The HAZ area is not significantly different from the parent metal, and needle-shaped silicones are clearly visible in it.

In order to more accurately examine different areas of the SZ region, the flow of material during the process was modeled. In order to study the process material flow, several places inside the stir zone are indicated (Fig. 8). It turns out that the tool rotates the bottom points from the front to the back of the tool probe, then causes them to return to their initial position. The top surface points, however, rotate with the tool probe and eventually expand in the direction of the advancing side. The stir zone also exhibits two distinct patterns of material flow with two distinct thermomechanical histories. The highest flow of material is produced in the shoulder-affected flow region, and as one moves further away from the joint's top surface, the flow of material rapidly diminishes. The material flow difference throughout the plates' depth may cause the basin-shaped stir zone that enlarges near the top surface.

5. Conclusion

A proper design of the FSW/FSP tool requires an understanding of the role that each component of the probe and shoulder of the tool plays in the generation of heat and strain. To study the role of the tool probe and shoulder on heat and strain production, processes employed a tool without a probe, a tool without a shoulder, and an FSW tool were numerically simulated using a thermo-mechanically coupled three-dimensional FEM model. As a result, the following conclusions were reached.

- In the probeless tool, the maximum temperature is 390°, which is about 90% of the temperature of the joint produced with the FSW/FSP tool. A probeless tool produces a lower temperature than an FSW/FSP tool, which indicates that most of the heat is generated by the tool shoulder.

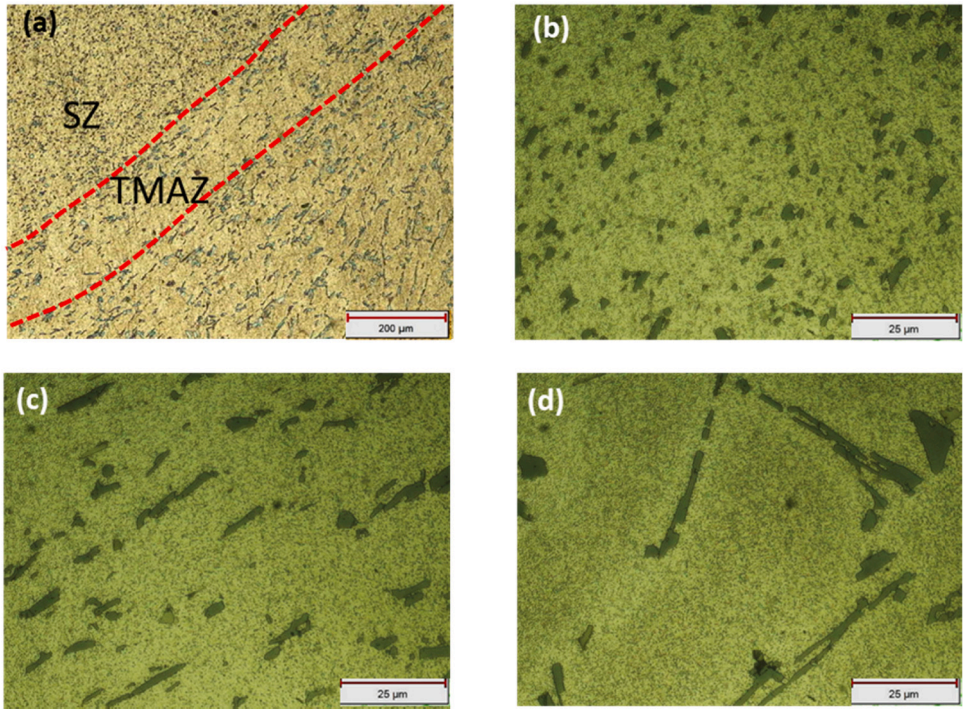

Fig. 7. The microstructure of (a) welding zone, (b) SZ, (c) TMAZ, (d) parent alloy.

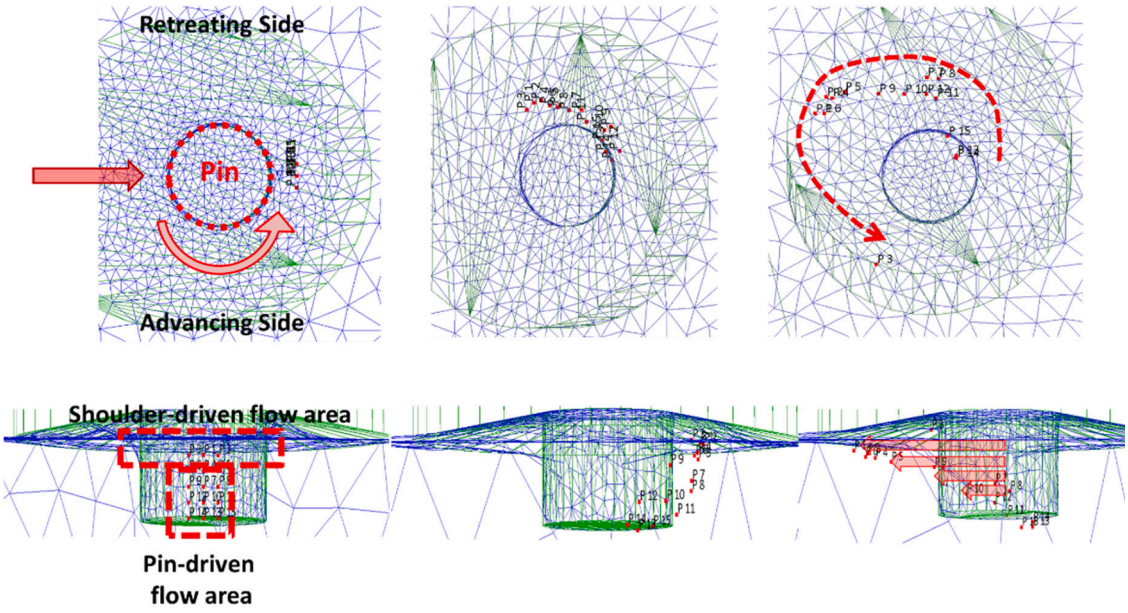

Fig. 8. Material flow pattern in FSW process.

- The findings indicate that frictional heat generation is the predominant mechanism for raising workpiece temperature in contrast to plastic deformation.
- There is only a small increase in temperature around the probe in the joint produced with the shoulderless tool compared to the one produced with the FSW/FSP tool.
- FSW/FSP samples have a much higher strain due to the combination of shoulder and probe effects than shoulderless or probeless samples.
- There is a maximum strain at the intersection of the area under the influence of the probe and the area under the influence of the shoulder.
- The shoulderless tool was unable to create strain in the material due to insufficient heat generation by the shoulder of the tool.

Declaration of Competing Interest

The authors declare no competing interests.

Data availability

No data was used for the research described in the article.

References

[1] M. Akbari, A. Khalkhali, S.M.E. Keshavarz, et al., Investigation of the effect of friction stir processing parameters on temperature and forces of Al–Si aluminum alloys, Proc. Inst. Mech. Eng. L J. Mater. Des. Appl. 232 (2015) 213–229, https://doi.org/10.1177/1464420715621337.

[2] M. Akbari, A. Khalkhali, S.M.E. Keshavarz, et al., The effect of in-process cooling conditions on temperature, force, wear resistance, microstructural, and mechanical properties of friction stir processed A356, Proc. Inst. Mech. Eng. L J. Mater. Des. Appl. 232 (2016) 429–437, https://doi.org/10.1177/1464420716630569.

[3] M. Cabibbo, E. Meccia, E. Evangelista, TEM analysis of a friction stir-welded butt joint of Al–Si–Mg alloys, Mater. Chem. Phys. 81 (2003) 289–292, https://doi.org/10.1016/S0254-0584(02)00604-1.

[4] P. Zolghadr, M. Akbari, P. Asadi, Formation of thermo-mechanically affected zone in friction stir welding, Mater. Res. Exp. 6 (2019), 086558, https://doi.org/10.1088/2053-1591/ab1d25.

[5] P. Asadi, M.R.M. Aliha, M. Akbari, et al., Multivariate optimization of mechanical and microstructural properties of welded joints by FSW method, Eng. Fail. Anal. 140 (2022), 106528, https://doi.org/10.1016/j.engfailanal.2022.106528.

[6] A. Ghiasvand, M. Kazemi, M. Mahdipour Jalilian, et al., Effects of tool offset, pin offset, and alloys position on maximum temperature in dissimilar FSW of AA6061 and AA5086, Int. J. Mech. Mater. Eng. 15 (6) (2020), https://doi.org/10.1186/s40712-020-00118-y.

[7] S.D. Dhanesh Babu, P. Sevvel, R. Senthil Kumar, et al., Development of thermo mechanical model for prediction of temperature diffusion in different FSW tool pin geometries during joining of AZ80A Mg alloys, J. Inorg. Organomet. Polym. Mater. 31 (2021) 3196–3212, https://doi.org/10.1007/s10904-021-01931-4.

[8] M. Akbari, P. Asadi, R.A. Behnagh, Modeling of material flow in dissimilar friction stir lap welding of aluminum and brass using coupled Eulerian and Lagrangian method, Int. J. Adv. Manuf. Technol. 113 (2021) 721–734, https://doi.org/10.1007/s00170-020-06541-x.

[9] M. Akbari, P. Asadi, Effects of different cooling conditions on friction stir processing of A356 alloy: numerical modeling and experiment, Proc. Inst. Mech. Eng. C J. Mech. Eng. Sci. 236 (2021) 4133–4146, https://doi.org/10.1177/0954406221104565.

[10] C. Ranjole, V.P. Singh, B. Kuriachen, et al., Numerical prediction and experimental investigation of temperature, residual stress and mechanical properties of dissimilar friction-stir welded AA5083 and AZ31 alloys, Arab. J. Sci. 47 (2022) 16103–16115, https://doi.org/10.1007/s13369-022-06808-3.

[11] N. Sharma, A.N. Siddiquee, Z.A. Khan, et al., Material stirring during FSW of Al–Cu: effect of pin profile, Mater. Manuf. Process. 33 (2018) 786–794, https://doi.org/10.1080/10426914.2017.1388526.

[12] P.S. Kumar, M.S. Chander, Effect of tool pin geometry on FSW dissimilar aluminum alloys - (AA5083 & AA6061), Mater. Today Proc. 39 (2021) 472–477, https://doi.org/10.1016/j.matpr.2020.08.204.

[13] K. Krasnowski, C. Hamilton, S. Dymek, Influence of the tool shape and weld configuration on microstructure and mechanical properties of the Al 6082 alloy FSW joints, Arch. Civ. Mech. Eng. 15 (2015) 133–141, https://doi.org/10.1016/j.acme.2014.02.001.

[14] G. Padmanaban, V. Balasubramanian, Selection of FSW tool pin profile, shoulder diameter and material for joining AZ31B magnesium alloy – an experimental approach, Mater. Des. 30 (2009) 2647–2656, https://doi.org/10.1016/j.matdes.2008.10.021.

[15] M.H. Shojaeefard, A. Khalkhali, M. Akbari, et al., Investigation of friction stir welding tool parameters using FEM and neural network, Proc. Inst. Mech. Eng. L J. Mater. Des. Appl. 229 (2013) 209–217, https://doi.org/10.1177/1464420713509075.

[16] M.K. Kulekci, A. Şik, E. Kaluç, Effects of tool rotation and pin diameter on fatigue properties of friction stir welded lap joints, Int. J. Adv. Manuf. Technol. 36 (2008) 877–882, https://doi.org/10.1007/s00170-006-0901-z.

[17] M. Akbari, M.R.M. Aliha, S.M.E. Keshavarz, et al., Effect of tool parameters on mechanical properties, temperature, and force generation during FSW, Proc. Inst. Mech. Eng. L J. Mater. Des. Appl. 233 (2016) 1033–1043, https://doi.org/10.1177/1464420716681591.

[18] S. Shashi Kumar, N. Murugan, K.K Ramachandran, Influence of tool material on mechanical and microstructural properties of friction stir welded 316L austenitic stainless steel butt joints, Int. J. Refract. Met. Hard Mater. 58 (2016) 196–205, https://doi.org/10.1016/j.ijrmhm.2016.04.015.

[19] P. Asadi, R.A. Mahdavinejad, S. Tutunchilar, Simulation and experimental investigation of FSP of AZ91 magnesium alloy, Mater. Sci. Eng. A 528 (2011) 6469–6477, https://doi.org/10.1016/j.msea.2011.05.035.

[20] S. Tutunchilar, M. Haghpanahi, M.K. Besharati Givi, et al., Simulation of material flow in friction stir processing of a cast Al–Si alloy, Mater. Des. 40 (2012) 415–426, https://doi.org/10.1016/j.matdes.2012.04.001.

[21] M. Assidi, L. Fourment, S. Guerdoux, et al., Friction model for friction stir welding process simulation: calibrations from welding experiments, Int. J. Mach. Tools Manuf. 50 (2010) 143–155, https://doi.org/10.1016/j.ijmachtools.2009.11.008.

[22] P. Asadi, M. Akbari, H. Karimi-Nemch, M.K.B. Givi, P. Asadi, 12 - Simulation of friction stir welding and processing. Advances in Friction-Stir Welding and Processing, Woodhead Publishing, 2014, pp. 499–542.
[23] J. Marzbanrad, M. Akbari, P. Asadi, et al., Characterization of the influence of tool pin profile on microstructural and mechanical properties of friction stir welding, Metall. Mater. Trans. B. 45 (2014) 1887–1894, https://doi.org/10.1007/s11663-014-0089-9.
[24] Shojaeefard, M.H., Khalkhali, A., Akbari, M. et al., Investigation of friction stir welding tool parameters using FEM and neural network, Proc. Inst. Mech. Eng. L J. Mater. Des. Appl. 229(3) (2015) 209-217, doi:10.1177/1464420713509075 (2013).
[25] P. Asadi, M. Besharati Givi, M. Akbari, Microstructural simulation of friction stir welding using a cellular automaton method: a microstructure prediction of AZ91 magnesium alloy, Int. J. Mech. Mater. Eng. 10 (2015) 1–14, https://doi.org/10.1186/s40712-015-0048-5.
[26] M. Shojaeefard, M. Akbari, P. Asadi, Multi objective optimization of friction stir welding parameters using FEM and neural network, Int. J. Precis. Eng. Manuf. 15 (2014) 2351–2356, https://doi.org/10.1007/s12541-014-0600-x.
[27] M.H. Shojaeefard, M. Akbari, A. Khalkhali, et al., Optimization of microstructural and mechanical properties of friction stir welding using the cellular automaton and Taguchi method, Mater. Des. 64 (2014) 660–666, https://doi.org/10.1016/j.matdes.2014.08.014.
[28] P. Asadi, M.K.B. Givi, A. Rastgoo, et al., Predicting the grain size and hardness of AZ91/SiC nanocomposite by artificial neural networks, Int. J. Adv. Manuf. Technol. 63 (2012) 1095–1107, https://doi.org/10.1007/s00170-012-3972-z.
[29] P. Asadi, M. Besharati Givi, M. Akbari, Simulation of dynamic recrystallization process during friction stir welding of AZ91 magnesium alloy, Int. J. Adv. Manuf. Technol. (2015) 1–11, https://doi.org/10.1007/s00170-015-7595-z.